Accepted Manuscript

Evaluation of polyesteramide (PEA) and polyester (PLGA) microspheres as intravitreal drug delivery systems in albino rats

Tobias Peters, Seong-Woo Kim, Vinicius Castro, Krunoslav Stingl, Torsten Strasser, Sylvia Bolz, Ulrich Schraermeyer, George Mihov, MengMeng Zong, Vanessa Andres-Guerrero, Rocio Herrero Vanrell, Aylvin A. Dias, Neil R. Cameron, Eberhart Zrenner

PII: S0142-9612(17)30074-1

DOI: 10.1016/j.biomaterials.2017.02.006

Reference: JBMT 17935

To appear in: *Biomaterials*

Received Date: 24 November 2016

Revised Date: 20 January 2017

Accepted Date: 6 February 2017

Please cite this article as: Peters T, Kim S-W, Castro V, Stingl K, Strasser T, Bolz S, Schraermeyer U, Mihov G, Zong M, Andres-Guerrero V, Herrero Vanrell R, Dias AA, Cameron NR, Zrenner E, Evaluation of polyesteramide (PEA) and polyester (PLGA) microspheres as intravitreal drug delivery systems in albino rats, *Biomaterials* (2017), doi: 10.1016/j.biomaterials.2017.02.006.

Evaluation of polyesteramide (PEA) and polyester (PLGA) microspheres as intravitreal drug delivery systems in albino rats

Tobias Peters[1,7], Seong-Woo Kim[2,7], Vinicius Castro[1], Krunoslav Stingl[1], Torsten Strasser[1], Sylvia Bolz[1], Ulrich Schraermeyer[1], George Mihov[3], MengMeng Zong[3], Vanessa Andres-Guerrero[5], Rocio Herrero Vanrell[5], Aylvin A Dias[3], Neil R. Cameron[6], Eberhart Zrenner[1,4]

[1] Institute for Ophthalmic Research at the Centre for Ophthalmology, University of Tübingen, Germany

[2] Department of Ophthalmology, Korea University College of Medicine, Seoul, Korea

[3] DSM, Urmonderbaan 22, Geleen, Netherlands

[4] Werner Reichardt Centre for Integrative Neuroscience (CIN) and Centre for Ophthalmology, University of Tübingen, Germany

[5] Sanitary Research Institute of the San Carlos Clinical Hospital, Department of Pharmacy and Pharmaceutical Technology, Faculty of Pharmacy, Complutense University of Madrid, Spain

[6] Department of Chemistry, University of Durham, United Kingdom

[7] Equally shared First-Authorship

Financial support: The project is supported by funding from the Nanosciences, Nanotechnologies, Materials & New Production Technologies (NMP) Theme of the

Cooperation Program, under the 7th Research Framework Program of the European Union (PANOPTES project, project number 246180).

Tistou and Charlotte Kerstan Foundation to Torsten Strasser and Seong-Woo Kim, Deutsche Forschungsgemeinschaft (DFG) EXC 307 to Eberhart Zrenner

Conflict of Interest: The authors from DSM have proprietary and commercial interest in material discussed in this article. All other authors: none

Equally shared First-Authorship: Seong Woo Kim and Tobias Peters

Corresponding author: Tobias Peters, tobias.peters@uni-tuebingen.de

Key words: poly ester amide based on α-amino acids, aliphatic dicarboxylic acids and aliphatic α-ω diols (PEA), poly lactic-co-glycolic acid (PLGA), invivo electroretinography, invivo optical coherence tomography, fundus auto-fluorescence, immunohistochemistry, TUNEL stain, transmission electron microscopy

Abstract

Purpose: To study the suitability of injectable microspheres based on poly(ester amide) (PEA) or poly lactic-co-glycolic acid (PLGA) as potential vehicles for intravitreal drug delivery in rat eyes. Dexamethasone-loaded PEA microspheres (PEA+DEX) were also evaluated.

Methods: Forty male Sprague Dawley rats were divided into four groups that received different intravitreally injected microspheres: PEA group (n=12); PLGA group (n=12); PEA+DEX group (n=8); and control group (no injection, n=8). Electroretinography (ERG), fundus autofluorescence (FAF), and spectral domain optical coherence tomography (sdOCT) were performed at baseline, weeks 1 and 2, and months 1, 2, and 3 after intravitreal injection. Eyes were histologically examined using light microscopy and transmission electron microscopy at the end of the in vivo study.

Results: There were no statistically significant changes in ERG among the groups. Abnormal FAF pattern and abnormal deposits in OCT were observed after injection but almost completely disappeared between week 2 and month 3 in all injected groups. GFAP staining showed that Müller glia cell activation was most pronounced in PLGA-injected eyes. Increased cell death was not observed by TUNEL staining at month 1. In electron microscopy at month 3, the remnants of microparticles were found in the retinal cells of all injected groups, and loss of plasma membrane was seen in the PLGA group.

Conclusions: Although morphological changes such as mild glial activation and material remnants were observed histologically 1 month and 3 months after injection

in all injected groups, minor cell damage was noted only in the PLGA group at 3 months after injection. No evidence of functional abnormality relative to untreated eyes could be detected by ERG 3 months after injection in all groups. Changes observed in in vivo imaging such as OCT and FAF disappeared after 3 months in almost all cases.

Recently, sustained intraocular drug delivery systems have received great attention because they can release the drug over a long time with only a single administration, thus avoiding the requirement for repeated multiple injections to maintain therapeutic drug levels, through their ability to cross the blood-ocular barrier. Biodegradable polymers have the additional advantage of disappearing from the vitreous after releasing the drug [1]. Currently, among the biodegradable polymers used to prepare drug delivery systems, poly lactic-co-glycolic acid (PLGA, [2]) is most widely used for various vitreoretinal diseases such as age-related macular degeneration, diabetic macular edema, and uveitis [3-9]. Biodegradable polyesteramides are a new class of biomaterials that show promise for medical applications, including drug delivery [10]. Amino acid-based polyesteramides (PEAs) are a new family of biodegradable polymers based on alpha-amino acids, aliphatic dicarboxylic acids, and aliphatic α-ω diols [11]. Incorporation of amino acid-based building blocks not only provides metabolizable degradation products [10], but also offers one or more functional groups along the polymer chain. This allows further modification of the polymer to tailor its physicochemical properties, degradation properties [12,13], and performance as a drug eluting matrix. In addition to good biocompatibility properties [14], the PEA material platform offers novel attractive features of particular interest for drug delivery [15,16]. PEA polymers are well tolerated in vivo and can be easily processed to yield a variety of medical device coatings [17], micron-sized implants, and particles [16]. Additionally, the polymer backbone undergoes enzymatic degradation via a unique surface erosion mechanism that does not produce changes in local pH [1,18]. This class of polymers has recently been explored as a drug delivery vehicle in a variety of ophthalmologic

therapies. The current paper focuses on the tolerability of PEA microparticles in the eye vitreous. Particle biocompatibility is benchmarked versus medical grade PLGA – a biomaterial known for its good biocompatibility and degradability in physiological environments. In the present study, microspheres containing PEA, PLGA, and PEA plus dexamethasone (PEA+DEX) were administered intravitreally in addition to a no-injection control, and all groups were assessed in terms of functional and morphologic alterations of the retina by electroretinography (ERG), *in vivo* imaging by fundus autofluorescence (FAF), spectral domain optical coherence tomography (sdOCT), and histology (immunohistochemistry, TUNEL assay, and transmission electron microscopy (TEM)) in the albino rat eye.

Materials

The PEA polymer in this work is random co-polymer comprising three di-amino building blocks randomly connected by di-acid to form the polymer chain and prepared by the Department of Pharmacy and Pharmaceutical Technology, Faculty of Pharmacy, Complutense University of Madrid, Spain.

Polyesteramide (PEA III Ac Bz, Mn = 49 kDa, PDI =1,56, Tg = 49°, provided by DSM, Geleen, Netherlands) and Poly-(D,L-lactide-co-glycolide) Mn = 35 kDa (PLGA ratio 50:50; Resomer® 503, Boehringer Ingelheim, Germany) microspheres were prepared based on the emulsion solvent-evaporation technique, as described in Andrés-Guerrero et al. [19,20]. Briefly, an organic phase composed of the polymer (PEA or PLGA) and dichloromethane (DCM) was emulsified (Polytron PT3000, Kinematica, Lucerna, Switzerland) with an aqueous solution of polyvinyl alcohol 67 kDa (PVA; Merck (Darmstadt, Germany). Then, the resulting emulsion was kept under constant stirring to allow organic solvent evaporation and hardening of

microspheres. In a final step, microspheres were washed, filtered and freeze-dried to obtain solid microspheres. To prepare drug-loaded microspheres, dexamethasone (DX) was dispersed in an organic phase composed by PEA and DCM at a ratio 2:10, followed by the rest of the steps described for the formation of non-loaded microspheres.

Microspheres were imaged through scanning electron microscopy to visualize their ultrastructure (SEM; Jeol JSM-6335F, Tokyo, Japan). Mean particle size and particle size distribution were measured by light scattering in a Microtrac S3500 Series Particle Size Analyzer (Montgomeryville, PA, USA). Data are presented as mean volume diameter ± standard deviation of three independent measurements.

The encapsulation efficiency of DX in PEA microspheres and the in vitro release studies of solid DX-PEA Microspheres were determined by high performance liquid chromatography (HPLC; Pump M520, UV detector M490E, autosampler 712D WTSP and the Empower Login HPLC System Manager Software), as previously described [19]. The method was validated with respect to linearity, accuracy and reliability in the range of concentrations of 2-20 µg/mL, for both the evaluation of the encapsulation efficiency (determined in a mixture of DCM/ACN) and the in vitro release study (performed in release media). Succinctly, to analyze drug content, 5 mg of DX loaded PEA microspheres were dissolved in DCM (0.2 mL) and diluted in ACN (0.8 mL), followed by a centrifugation (15,000 rpm, 4ºC, 15 min) and filtration (0.45 µm membrane) process. For the in vitro release studies, 5 mg of solid DX-PEA microspheres were incubated in a phosphate buffered solution isotonized with sodium chloride (PBS, pH 7.4) under sink conditions. Samples were placed in a water bath at 37ºC, being constantly shacked (100 rpm). At pre-set times (1h, 24h

and twice every week during 90 days) the supernatant was collected and analyzed by HPLC as described below (the study was performed in triplicate).

Microspheres characterization

The preparation process yielded round microspheres with smooth surface. Mean particle size of microspheres ranged between 10 to 20 µm (13.1 ± 7.1 µm for blank PEA microspheres, 14.9 ± 6.4 µm for DX-loaded PEA microspheres and 19.2 ± 6.1 µm for PLGA microspheres), optimum to be administered as an aqueous suspension by intravitreal injection through standard needles (27-34G) (Supplementary Fig. 1). The encapsulation efficiency of DX was around 85% (181.2 ± 2.4 µg DX/mg microspheres, respectively). DX-loaded PEA microspheres are capable of providing a sustained release of DX for at least 90 days. The release was characterized by an initial burst of 17.3 ± 0.4 µg DX/mg microspheres (9.4 ± 0.3%) during the first 24 h, followed by a short rapid release period of one week and a second long period of slow release up to 90 days. The cumulative release of the drug was around 54.4% of the encapsulated active substance (99.5 µg DX/mg Microspheres) at the end of the release assay (day 90). The degradation properties of PEA III Ac Bz are described previously [11,14,21,23]

Methods

Forty male Sprague Dawley rats (age: 15–16 weeks, breeder: Charles River Laboratories Inc., Sulzfeld, Germany) with a mean weight ± standard deviation (SD) of 301.78 ± 22.52 g at baseline were included. The animals were divided into four groups according to the intravitreally injected drug material: PEA group (n = 12); PLGA group (n = 12); PEA+DEX group (n = 8); control group (n = 8). Sterile microspheres suspended in 3 µl of sterile balanced salt solution (BSS; 25 mg/ml)

were injected via the pars plana of the right eye under a surgical microscope; the left eye did not receive any treatment and served as a control in functional analyses (ERG). For the PEA+DEX group, PEA microspheres were loaded with dexamethasone (181.0 ± 2.4 µg dexamethasone/mg PEA microspheres). The highest possible dexamethasone dose in the microsphere injection was approximately 13.6 µg (181 µg/mg * 25 mg/ml * 0.003 ml). The control group did not receive intravitreal injection in either eye. The microspheres were slowly injected for 30 seconds, and the elapsed time between injection and needle withdrawal from the eye was 30 seconds. All procedures and examinations were performed after intraperitoneal anesthesia with ketamine (100 mg/kg) and xylazine (5 mg/kg). ERG, FAF, and sdOCT were performed at six time points: 1 week before injection (baseline) and 1 week, 2 weeks, 1 month, 2 months, and 3 months after injection. Rats were sacrificed at month 1 for immunohistochemical and TUNEL staining (four rats each in the PEA and PLGA groups, two rats each in the PEA+DEX and control groups). Additionally, two rats of each group were sacrificed for TEM at month 3. The rats were housed under standard laboratory conditions with a 12-hour dark and light cycle under room illumination of intensity 25–70 lux at cage roof level and with free access to food and water. This study was approved by the Ethics Committee for Animal Research of the local authorities, and all procedures were performed according to institutional guidelines, European Union regulations for the use of animals in research, and the Association for Research in Vision and Ophthalmology Statement for the Use of Animals in Ophthalmic and Vision Research.

Electroretinography

ERGs were recorded using an Espion e2 electrophysiology system and a Ganzfeld stimulator Color Dome (Diagnosys LLC Inc., Middleton, USA). All ERGs were recorded after 12 hours of dark adaptation. The pupils were dilated using one drop of 0.5% tropicamide (Mydriatikum®, Stulln, Germany) 20 minutes before ERG measurement, and a heating plate kept the body temperature at approximately 38℃. Subcutaneous platinum needles served as a ground electrode in the tail and as a reference electrode placed in the forehead between the eyes; active electrodes were gold ring electrodes placed on the cornea, which was moistened with 2% methylcellulose. Impedances of the electrodes were measured at 25 Hz before the start of the test and were kept below 10 kOhm during the recording. Signals were filtered digitally using a band pass filter (0.3 to 300 Hz). The dark-adapted (scotopic) ERG protocol consisted of eight steps with increasing luminance of white flashes at 6,500 K (0.0001, 0.001, 0.01, 0.1, 1.0, 3.0, 10, and 100 cd.s/m^2) and 4 ms duration. Oscillatory potentials (OP) were derived from the response to 10.0 cd.s/m² by bandpass filtering between 75 and 300 Hz. All scotopic flashes were delivered without background illumination and with a constant interstimulus interval of 10 s for dim flashes and up to 45 s for bright flashes, starting at 0.1 cd.s/m², to ensure stable dark-adapted conditions. Responses were averaged to increase the stimulus-to-noise ratio (six times for dim flashes and two times for bright flashes).

The photopic ERG protocol consisted of an initial light adaptation phase for 5 minutes with background illumination of 34 cd/m^2 that was kept on during all single-flash and flicker stimuli. For single-flash response, two steps with 3 cd.s/m² and 30 cd.s/m^2 with 4 ms duration of single white flashes were chosen. Four flicker steps (5, 10, 15, 20 Hz) were applied with constant white flashes of 3 cd.s/m^2. An average of

two sweeps for single flashes and 30 sweeps for flicker stimulation were acquired. (Fig. 1).

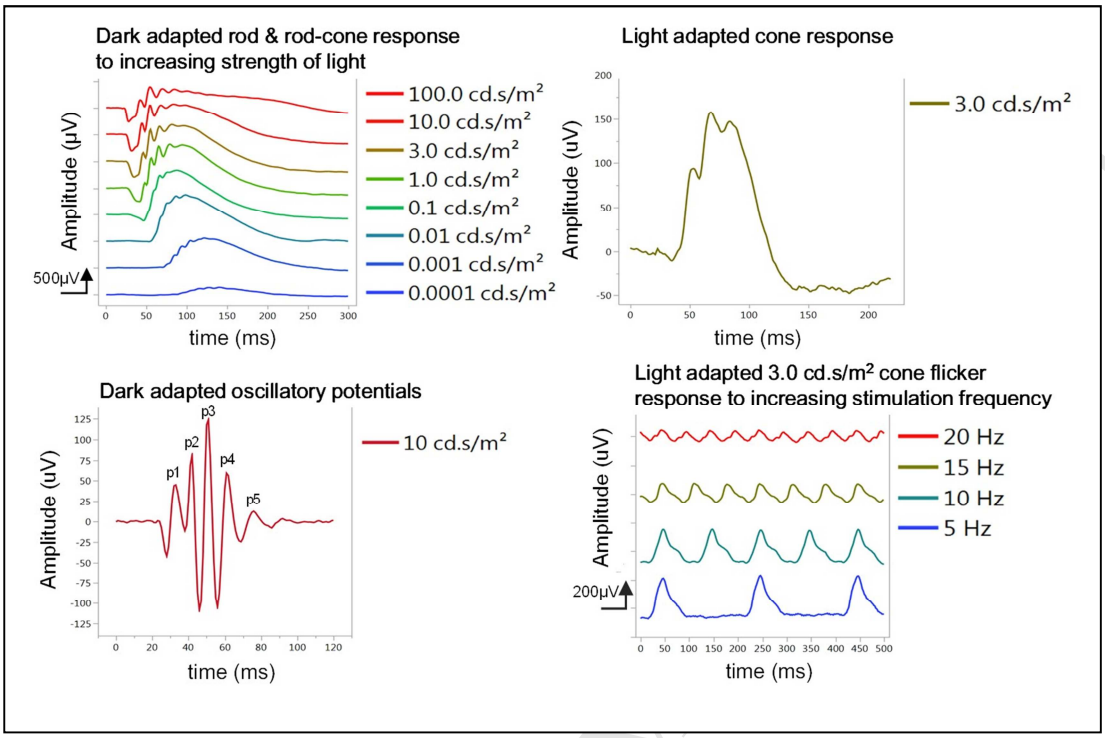

Figure 1. ERG response of healthy rat eye (OD) at baseline. Dark adapted a- and b-wave responses to eight flashes of increasing stimulus strength (0.0001–100 cd.s/m^2), oscillatory potentials, light-adapted cone response, and light-adapted cone flicker responses to four steps of increasing stimulus frequency (5–20 Hz).

In vivo retinal imaging

FAF and sdOCT were performed with a commercially available HRA+OCT Spectralis® device (Heidelberg Engineering Inc., Heidelberg, Germany) after ERG measurements. For adaptation to the optical qualities of the rat eye, a customized +3.25 diopter contact lens was used in front of the cornea. FAF and sdOCT images were acquired serially. The FAF images were acquired in both 30° and 55° field-of-

view. The FAF image resolution was 1,536 x 1,536 pixels, and a wavelength of 488 nm was used for excitation. Spectral domain OCT images included line, ring, and volume scans at 30°field-of-view. The number of A- scans per B-scan was 1,536. Optical depth resolution was approximately 7 µm, with digital resolution reaching 3.5 µm. The line scan was performed horizontally and vertically. The volume scan was performed with 31 B-scans. To obtain a high-quality mean image, up to 100 frames were averaged using the inbuilt automatic real-time (ART) algorithm.

Histology

Immunostaining for GFAP (gliofibrillary acidic protein, a major constituent of the astrocyte cytoskeleton) and IBA-1 (microglia/macrophage-specific ionized calcium-binding protein), terminal deoxynucleotidyl transferase dUTP nick end labeling (TUNEL) assay, and DAPI (4', 6-diamidino-2-phenylindole dihydrochloride) staining were performed in both eyes at month 1 (four rats in PEA and PLGA group, and two rats PEA+DEXA and control group). Eyes of two animals of each group were examined by TEM at month 3. After washing and embedding in tissue-freezing medium, eyecups were immediately fixed in 4% paraformaldehyde, frozen in liquid nitrogen, and cut in 12-µm serial sections. Detailed methods for tissue preparation, immunohistochemistry, TUNEL assay, and TEM are provided in the supplementary information.

Data analysis and statistics

Electrophysiological recordings were exported and pre-processed for

statistical analysis using ERG Explorer [24, 25]. Statistical analysis was performed using JMP® software (version 11.2.0 SAS institute, Cary, NC, USA). A two-way repeated analysis of variance (ANOVA) was conducted to compare the main effects of group and time on the electrophysiological responses. Group included four levels (PEA, PLGA, PEA+DEX, control), and time consisted of six levels (baseline, week 1, week 2, month 1, month 2, month 3). To reduce the influence of factors not related to the study question, such as interindividual differences and ERG measurement variability between different time points, statistical analysis was performed on the amplitude ratio (OD/OS) and on the implicit time (IT) difference (OD-OS), and each variable was compared to its own baseline. To compare oscillatory potentials (OP), the area under the curve (AUC) ratio (OD/OS) was measured. For analysis of the influence of different materials on the electrophysiological function of the retina, the following parameters were included in statistical analysis: dark-adapted single-flash responses at 0.001, 0.01, 3.0, 10, and 100 cd.s/m², dark-adapted OP at 10.0 cd.s/m², and light-adapted flicker response to 5, 10, 15, and 20 Hz. The selection of these parameters was determined with a focus on covering different subsystems of the retina: purely rod function (0.001 and 0.1 cd.s/m²), mixed rod-cone function (3.0, 10, and 100 cd.s/m²), purely cone function (light adapted flicker response), and function of inner retina (dark adapted oscillatory potentials). Multimodal mapper (MMM) software (Institute for Ophthalmic Research, University of Tuebingen, Tuebingen, Germany) [26] was used to quantify mean retinal thickness in ring scans of OCT. To acquire peripapillary retinal thickness (PRT) between the internal limiting membrane (ILM) and upper border of the retinal pigment epithelium (RPE) in the ring scan, the inner and outer borders were manually defined. The thickness at 38 equally spaced

points was measured automatically in the MMM software. Mean PRT was compared between the preinjection and postinjection periods. P values < 0.05 were considered statistically significant.

Results

None of the animals showed any signs of systemic adverse events or impairment over the course of the study. Weight gain during the study was in the normal range [27,28]. A total of 11 of 32 injected eyes developed localized posterior capsular opacity (cataract) along the injection needle direction (PEA group = 4/12, PLGA group = 5/12, PEA+DEX group = 2/8, Control group = N/A). One rat developed a retinal detachment after intravitreal injection. Three animals died in the course of the study for reasons not related to the treatment or any procedure (two rats developed pneumonia, and one rat did not recover from anesthesia).

Full-field electroretinography

No difference was found among the four groups in dark- or light-adapted ERG responses (amplitude ratio or implicit time difference) for all time points relative to baseline. There were no significant differences among the groups or in the interaction between time point and group, except the effects of the time factor on b-wave amplitude ratio (0.001 cd.s/m², $p = 0.008$) (Fig. 2A) and on b-wave implicit time difference (100 cd.s/m², $p = 0.034$) (Supplementary Fig. 2, Table 1). The b-wave

amplitude ratio and implicit time difference (dark-adapted 0.001 cd.s/m²) are shown in Figures 2A and 2B. The a-wave amplitude ratio and implicit time difference (dark-adapted 3.0 cd.s/m²) are shown in Figures 2C and 2D. The b-wave amplitude ratio and implicit time difference (dark-adapted 3.0 cd.s/m²) are shown in Figures 2E and 2F. The OP AUC ratio (10.0 cd.s/m²) for inner retina response is shown in Figure 2G. The 15 Hz flicker response (3.0 cd.s/m²) for light-adapted cone response is shown in Figure 2H.

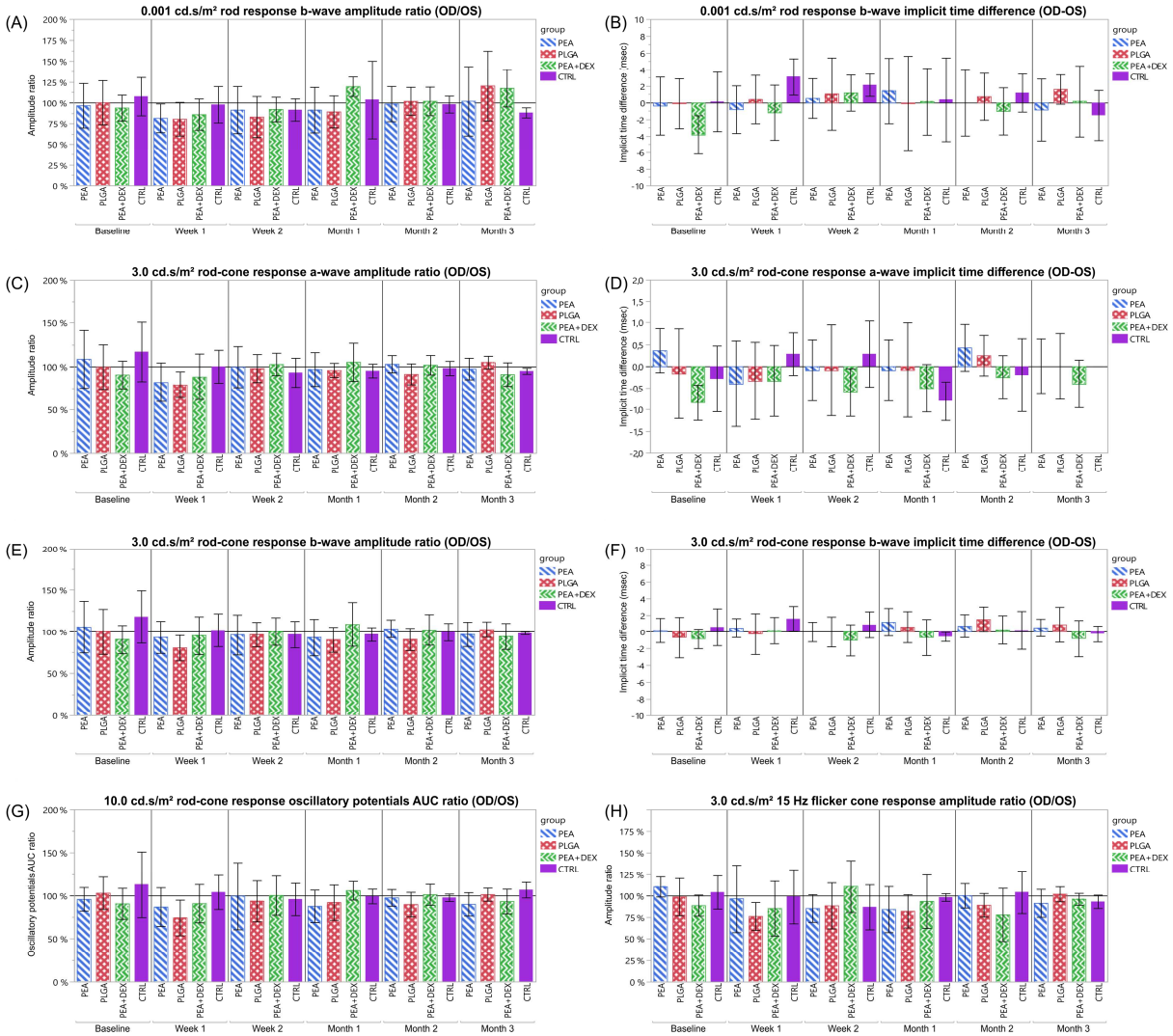

Figure 2. In the rod response to 0.001 cd.s/m², there was a significant effect of the

time factor in b-wave amplitude ratio (OD/OS) (p=0.008) (A) but not in b-wave implicit time difference (OD-OS) (B). In the rod-cone response to 3.0 cd.s/m², there was no significant effect of time or group in either a- or b-wave amplitude ratio (OD/OS) or implicit time difference (OD-OS) (C, D, E, F). In the rod-cone response to 10.0 cd.s/m², there was no significant effect of time or group on oscillatory potentials AUC ratio (OD/OS) (G). In the 15 Hz flicker response to 3.0 cd.s/m², there was no significant effect of time or group on amplitude ratio (OD/OS) (H).

Table 1. P values of amplitude ratio (OD/OS) and implicit time difference (OD-OS) response to light stimuli. All analyses included all time points using a two-way repeated measure analysis of variance (ANOVA) with within factor time and between factor groups.

	a-wave		b-wave	
Dark-adapted single-flash response	Amp ratio	IT diff	Amp ratio	IT diff
0.001 cd.s/m²	N/A	N/A	0.008	N/S
0.01 cd.s/m²	N/A	N/A	N/S	N/S
3.0 cd.s/m²	N/S	N/S	N/S	N/S
10 cd.s/m²	N/S	N/S	N/S	N/S
100 cd.s/m²	N/S	N/S	N/S	0.034
Oscillatory potentials area under the curve ratio				
10.0 cd.s/m²		N/S		
Light-adapted flicker response (amplitude ratio)				
5 Hz		N/S		
10 Hz		N/S		
15 Hz		N/S		
20 Hz		N/S		

Amp ratio = amplitude ratio; IT diff = implicit time difference; N/A = not applicable; N/S = not significant

In vivo retinal imaging

In vivo retinal imaging was hampered in a relatively large number of animals due to cataract and retinal detachment. Abnormal FAF finding was detected after intravitreal injection in 5/8 eyes in PEA group, 5/7 eyes in PLGA group, and 5/5 eyes in PEA+DEXA group. Abnormal FAF patterns were ring, patch, or mottled patterns (Table 2).

Table 2. Fundus autofluorescence findings

	Abnormal FAF pattern			OCT
Group (number*)	Patch (Fig. 4)	Mottled (Fig. 5)	Ring (Fig. 6)	Abnormal deposit
PEA group (n=8)	3	0	2	4
PLGA group (n=7)	2	1	2	4
PEA+DEX group (n=5)	0	3	2	5
Control group (n=7)	0	0	0	0

FAF = fundus autofluorescence; OCT = optical coherence tomography; PEA = poly (ester amide) based on α-amino acids, aliphatic dicarboxylic acids and aliphatic α-ω diols; PLGA = poly (lactic-co-glycolic acid); PEA+DEX = PEA plus dexamethasone.

* the available number of images was decreased due to cataract, retinal detachment, or death during follow-up.

Some animals developed abnormally increased FAF lesions in a circular pattern around the optic nerve (ring pattern) after intravitreal injection; this was most prominent at week 1 after injection, after which the intensity of abnormal FAF decreased. At the month 3 examination, the lesions had recovered or almost disappeared, and either very weak abnormal autofluorescence (AF) persisted or the

AF changed to a very subtle mottled pattern in 2/4 eyes in PEA group, 1/5 eyes in PLGA group, and 4/4 eyes in PEA+DEXA group (Figs. 3A, 4A, 5A, 6).

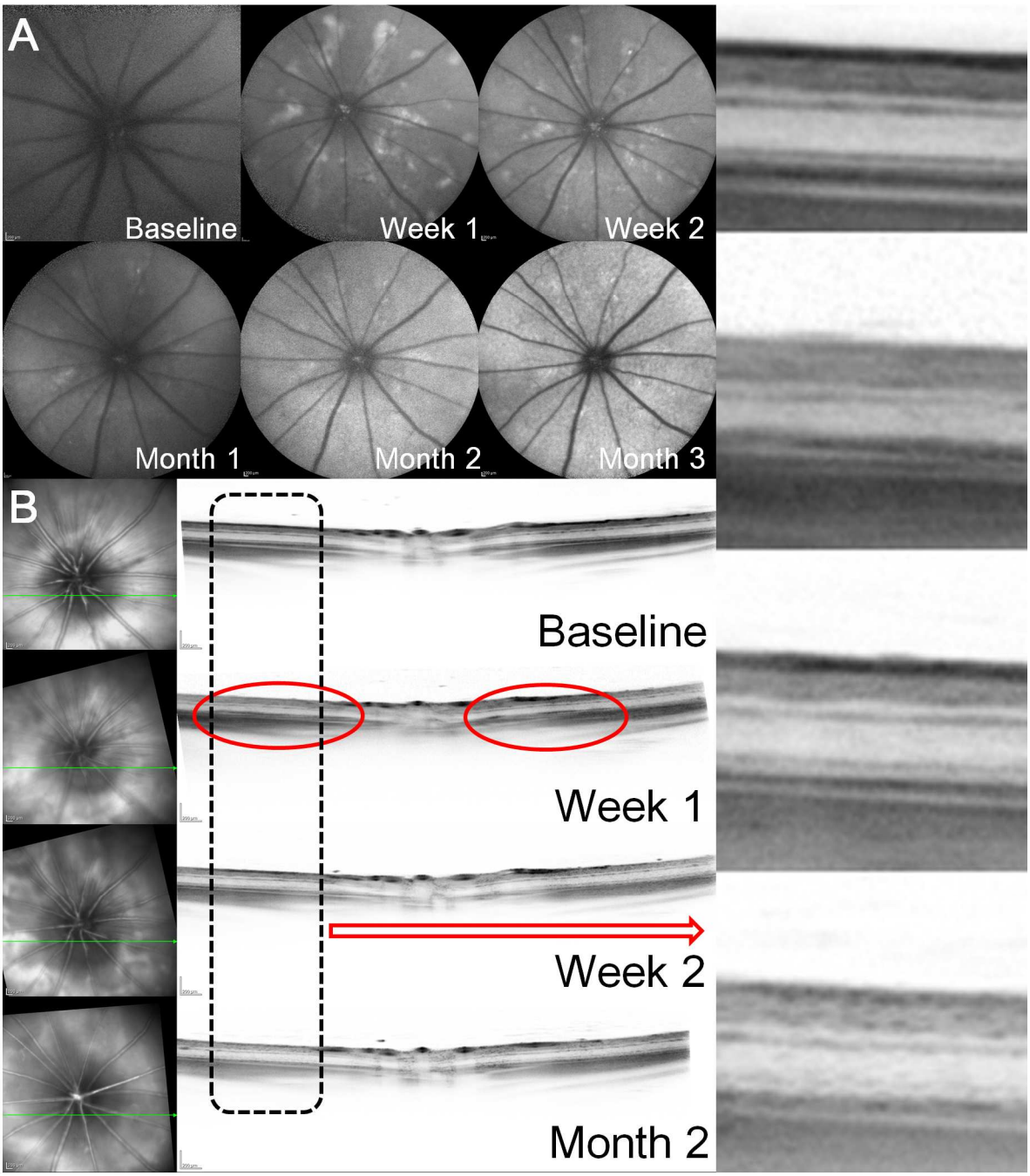

Figure 3. PEA-injected eye (rat number 6). (A) Fundus autofluorescence (AF) image

showed a patch pattern of hyper-AF areas at week 1 after intravitreal injection. The lesions gradually decreased and almost disappeared with time, but some remaining abnormal AF changes were still noted at month 3. (B) Optical coherence tomography image demonstrated abnormal linear deposit (red circle) proximal to the photoreceptor inner segment and outer segment (IS/OS) junction at week 1 after intravitreal injection. The IS/OS junction was discernible from the deposit. At week 2, the lesion had disappeared, and the normal retinal layer was visible again. By month 2, the retinal structure was intact.

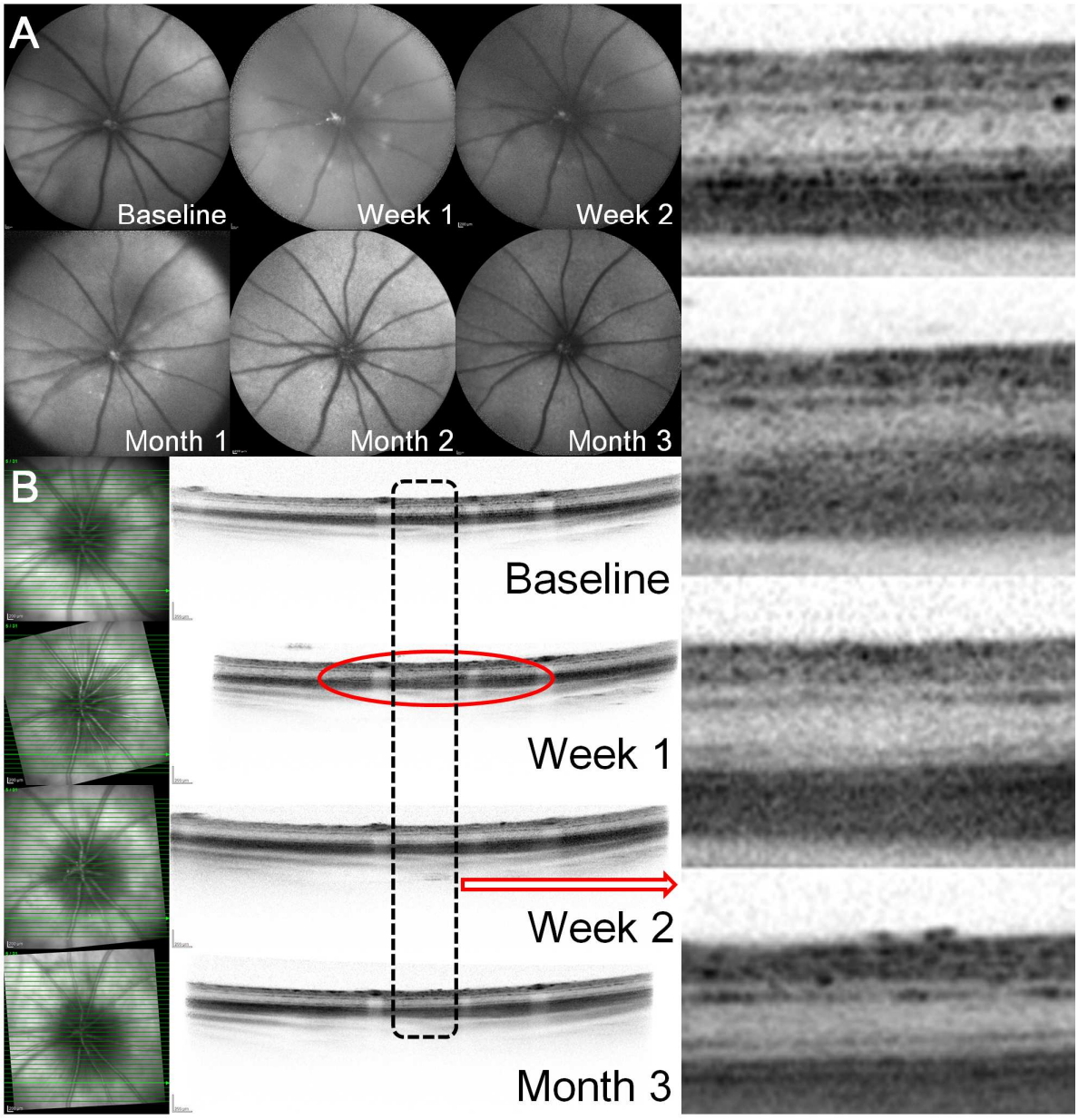

Figure 4. PLGA-injected eye (rat number 23). (A) Fundus autofluorescence (AF) image showed a mottled pattern of hyper-AF around the optic disc at week 1 after intravitreal injection. The lesion gradually decreased and disappeared by month 3. (B) At week 1 after intravitreal injection, optical coherence tomography image demonstrated abnormal linear deposit (red circle) proximal to the photoreceptor inner segment and outer segment junction, and the outer segment layer of photoreceptor

could not be differentiated from the deposit. At week 2, the lesion disappeared, and the normal retinal layer began to be visible again. By month 2, the retinal structure was intact.

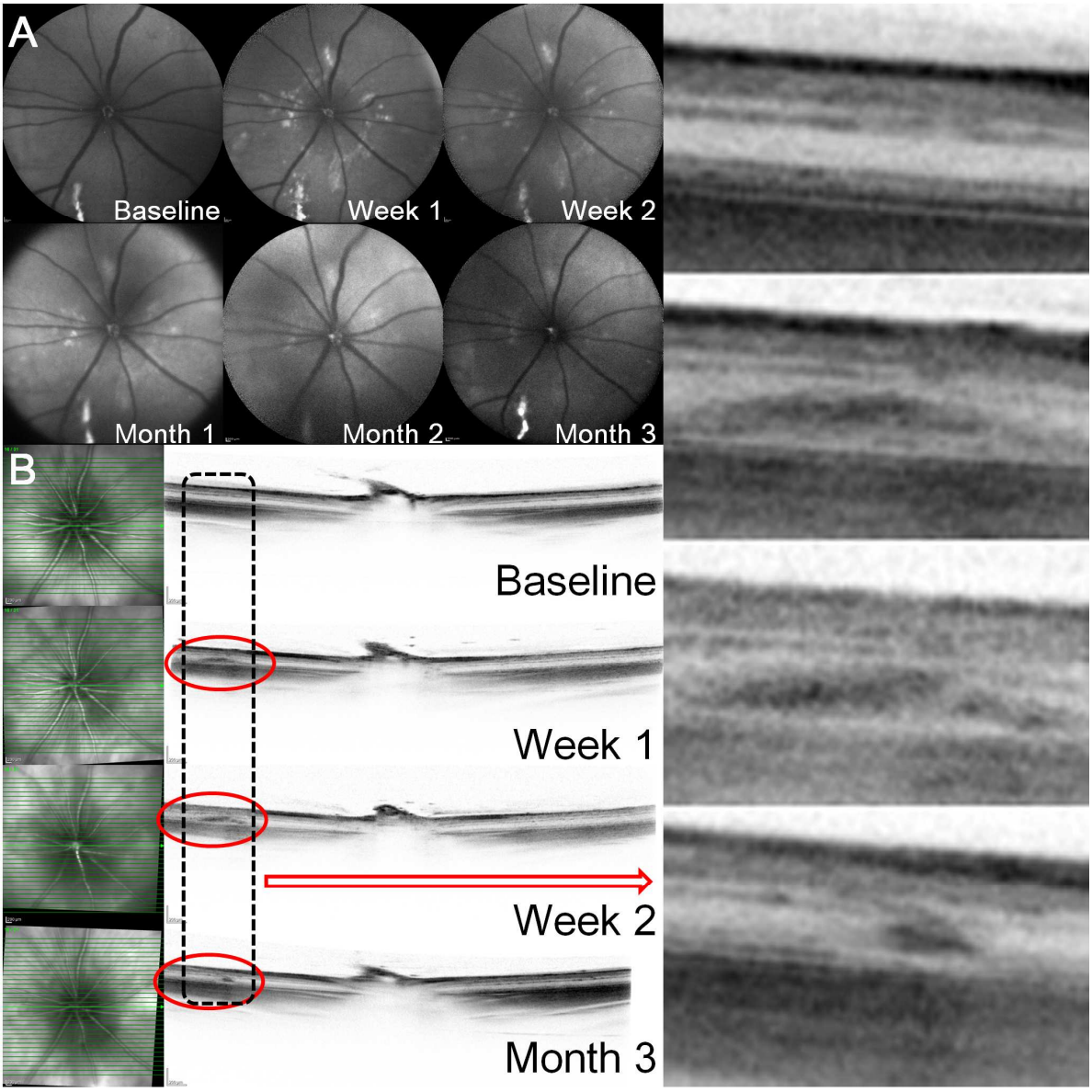

Figure 5. PEA+DEX injected eye (rat number 29). (A) Fundus autofluorescence (AF) image showed a ring pattern of hyper-AF around the optic disc from week 1 after intravitreal injection. The lesion gradually decreased and almost disappeared with time, but some remaining weak hyper-AF changes were still noted at month 3. (B)

Optical coherence tomography image demonstrated abnormal deposit (red circle) in the outer nuclear layer at week 1 after intravitreal injection. At week 2, the deposit had not disappeared. At month 3, the deposit was greatly decreased, and the intact retinal layer was appearing again even though minor deposits remained.

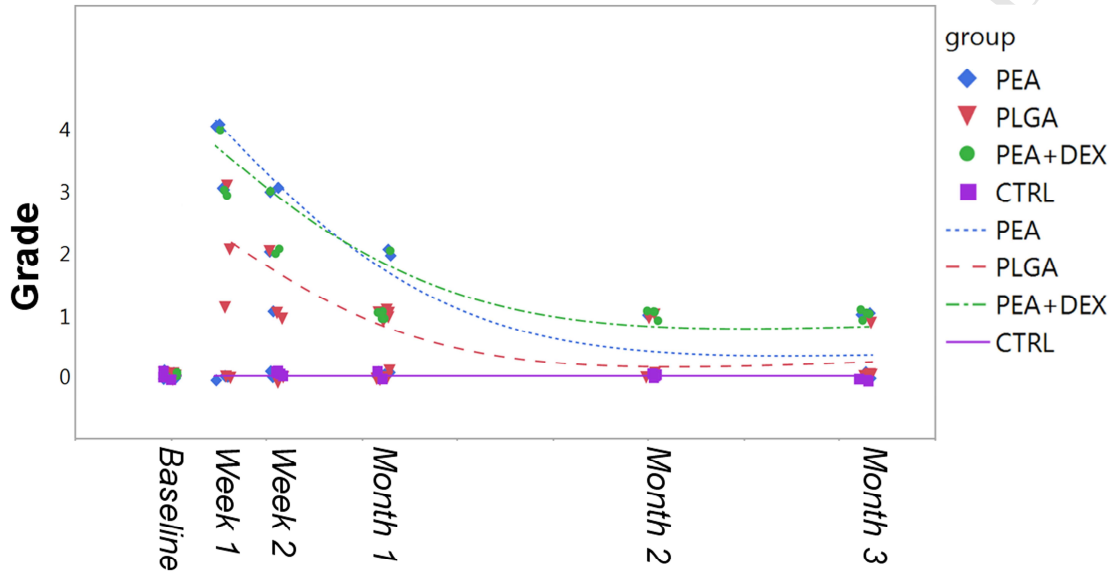

Figure 6. Change in fundus autofluorescence (AF) grade with time (Grade 0 = no abnormal AF, 1 = mild change, 2 = moderate, 3 = severe, 4 = very severe abnormal AF). Splines are fitted to indicate the trend in the data.

In the OCT image, abnormal linear deposits were noted over the photoreceptor inner segment and outer segment (IS/OS) junction or in the outer nuclear layer at week 1 after intravitreal injection. The IS/OS junction could be discerned from the deposit in some cases, while the outer segment layer of the

photoreceptor could not be separately differentiated from the deposit in the other cases. The lesion disappeared and the normal retinal layer was visible again in most cases at week 2, although minor retinal deposits remained inside the inner retina until month 3 (Figs. 3B, 4B, 5B). We could not find any significant change in PRT (Fig. 7).

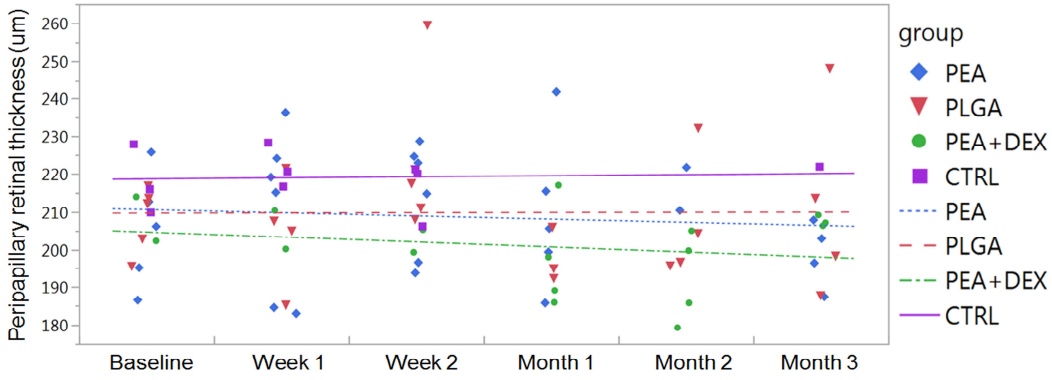

Figure 7. Change in peripapillary retinal thickness change (optical coherence tomography ring scan) with regression lines to indicate the trend in the data.

Histology

In 18 of 24 injected eyes examined, positive IBA-1 staining indicated microglial activation (Table 3).

Table 3. Overview of histopathological findings and immunohistochemical staining, (x/y = x of y animals)

	TUNEL positive	GFAP positive, up to axons	IBA positive, reaching inner retina
Right eye (injected)			
PEA	1/9	8/9	7/9
PLGA	0/10	8/10	8/10
PEA+DEX	0/5	4/5	3/5
Control	0/5	1/5	0/5
Left eye (control)			
PEA	0/9	1/9	1/9
PLGA	0/10	2/10	0/10
PEA+DEX	0/5	1/5	1/5
Control	0/5	1/5	0/5

TUNEL = terminal deoxynucleotidyl transferase dUTP nick end labeling; GFAP = anti-glial fibrillary acidic protein; IBA = anti-ionized calcium binding adapter molecule 1; PEA = poly (ester amide) based on α-amino acids, aliphatic dicarboxylic acids and aliphatic α-ω diols; PLGA = poly (lactic-co-glycolic acid); PEA+DEX = PEA plus dexamethasone.

The PEA+DEX-injected eyes showed lower activation of microglial cells than did the PEA- or PLGA-injected eyes. In GFAP staining, Müller glia cell activation was seen in 20 of 24 injected eyes, but also in two non-injected eyes. Müller cell activation was more pronounced in PLGA-injected eyes and less pronounced in PEA-injected eyes. TUNEL staining showed no increase in cell death for all eyes examined. Particles were distributed all over the retina, mostly on the surface of the ILM, although some particles were also seen in the inner retina up to the RPE layer (Fig. 8).

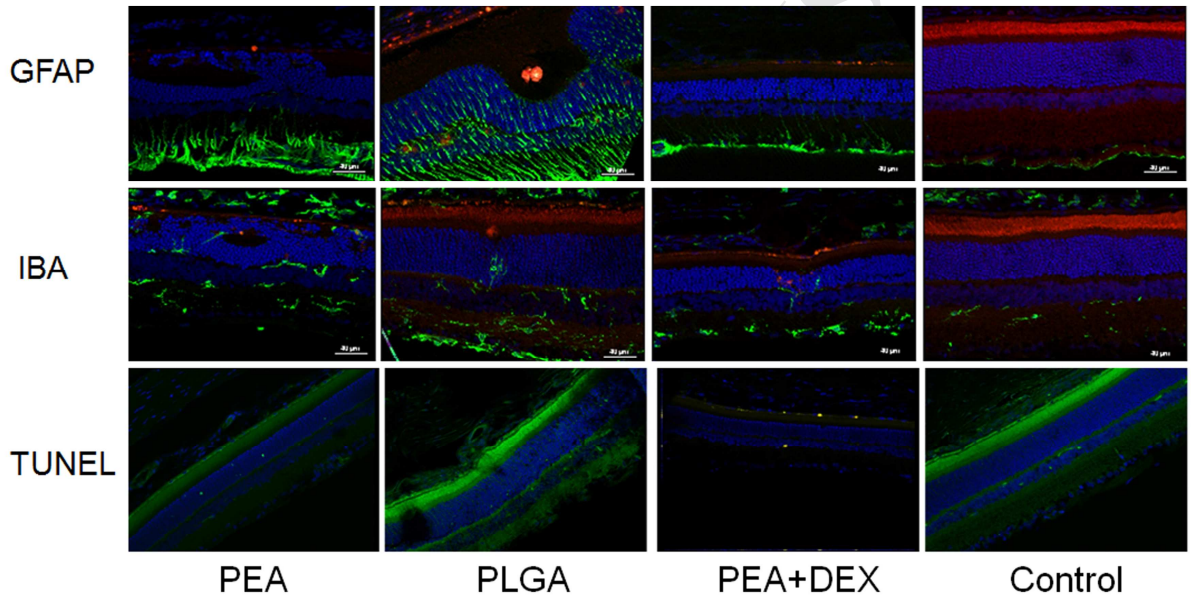

Figure 8. In immunohistochemical analysis at month 1, very prominent GFAP staining of Müller cells (green color) through the whole retina (from the ganglion cell layer [GCL] to external limiting membrane) was seen in the PLGA-injected eyes. In PEA+DEX-injected eyes, staining of GFAP was restricted to the Müller cell end feet and the GCL. In IBA staining, the PEA+DEXA-injected eyes showed milder activation of microglia than PEA- or PLGA-injected eyes. Microsphere particles were seen as red dots in GFAP and IBA staining. There was no TUNEL-positive staining that

would indicate increased cell death.

Transmission electron microscopy

TEM imaging performed in the right eye of two animals of each injected group at month 3 showed that the majority of microsphere particles were degraded. Remnants of degradation products of PEA were occasionally found in the basolateral space between RPE cells, basal labyrinth of RPE cells, blood vessels, and ganglion cells (Figs. 9A & 9B). In PLGA-injected eyes, degradation debris of PLGA was found in retinal cells, and loss of plasma membrane between two adjacent cells was observed (Figs. 9C & 9D).

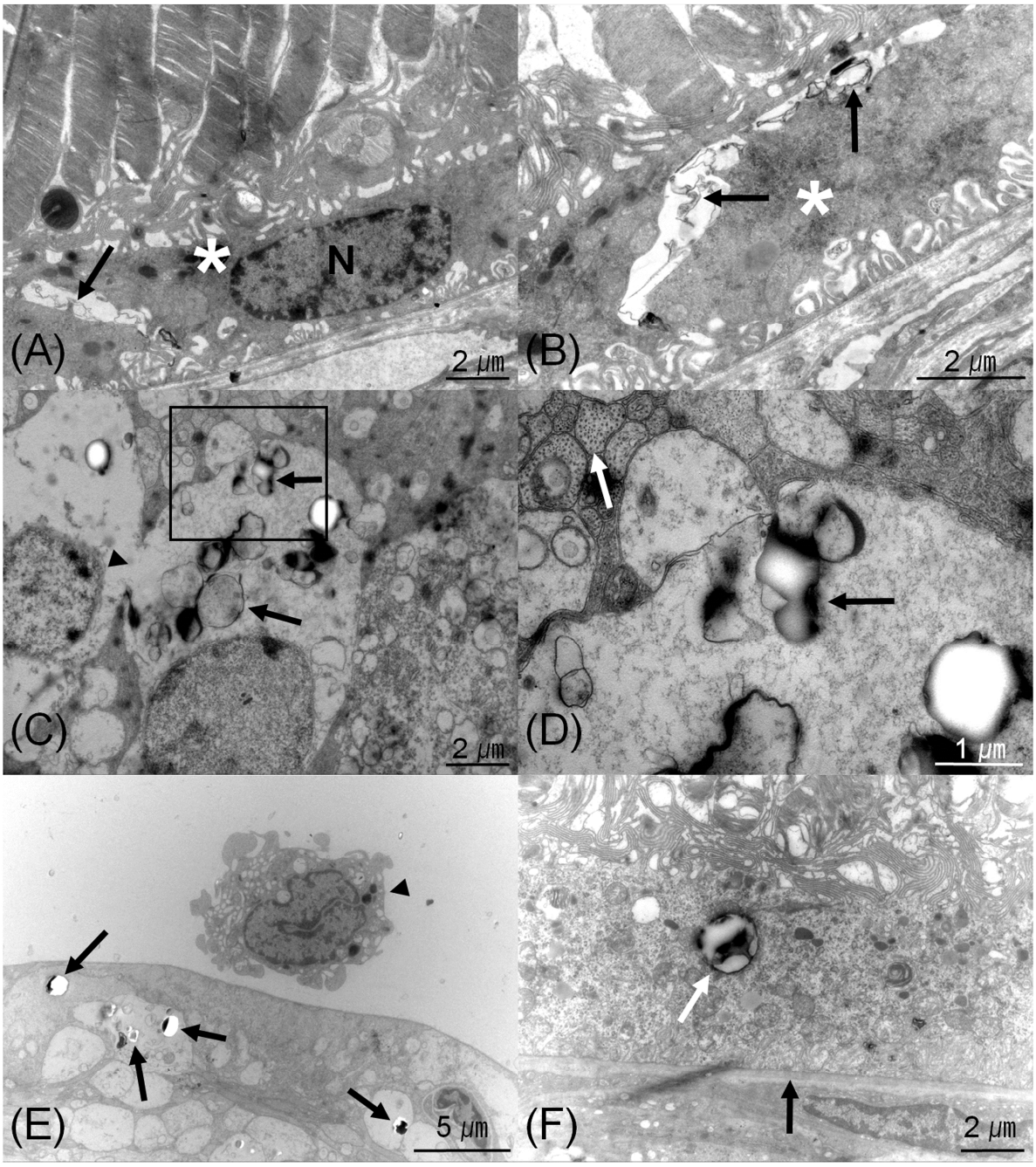

Figure 9. TEM imaging at month 3. In PEA-injected eyes (A, B), the basolateral spaces between retinal pigment epithelial (RPE) cells were enlarged and contained membranous materials (arrows) that were probably degradation products of PEA, as shown in an overview (A) and in detail (B). The RPE cell nucleus is indicated with N. The cytoplasm of RPE cells is marked by asterisks. In PLGA-injected eyes (C, D),

degradation products of PLGA were present in retinal ganglion cells (arrows). The plasma membrane between two adjacent cells was missing (arrowhead), indicating cell damage (C). The frame in C is shown at higher magnification in D. The degradation remnants of PLGA are marked by an arrow. The fixation was good because the neurotubles in the axons were very well preserved and could be clearly discriminated (white arrow) (D). In PEA+DEX-injected eyes (E, F), the remnants of PEA+DEX (arrows) were localized within retinal cells, and a macrophage (arrowhead) was visible in the vitreous close to the inner limiting membrane (E). The surface of these macrophages had many pseudopodia indicating activation, possibly induced by dexamethasone. Residual material of PEA+DEX (white arrow) is shown in a RPE cell (F). Bruch's membrane is labeled by an arrow.

Discussion

In the present study, three kinds of microspheres (PEA, PLGA, and PEA+DEX) were injected intravitreally, and their effects on eyes were compared with eyes of a control group using morphologic and functional examinations (OCT, FAF, ERG, and histology). None of the injected groups exhibited any signs of irreversible toxic effects over the course of the study. Rats were dosed intravitreally with 3 µl of microspheres at a given concentration of 5mg/mL, which was the most appropriate volume of PEA microspheres for intravitreal injection in the rat vitreous humor without increasing intraocular pressure.

Full-field electroretinography

In the present study, we did not find any statistically significant effect of time, group, or interaction between these two factors, indicating that the injected material did not lead to any changes in ERG amplitudes or implicit times in rod-only, rod-cone, or cone-only responses, with the exception of the b-wave amplitude ratio (OD/OS) response to 0.001 cd.s/m² and the b-wave implicit time difference (OD-OS) response to 100 cd.s/m^2. The absolute change in comparison of right (treated) and left (non-treated) eyes was less than 20% for the b-wave amplitude ratio (OD/OS) response to 0.001 cd.s/m² and less than 3% for the b-wave implicit time difference (OD-OS) response to 100 cd.s/m^2 and therefore of no clinical relevance [29]. The number of parameters included in the statistical analysis (Table 1) with an alpha value of 0.05 indicates that these findings are most possibly attributed to a type I error. An alternative explanation could be the transient influence of the intravitreal injection itself. These time/amplitude differences were mostly generated by a slight increase in implicit time of about 2 ms or decreased amplitude in an already very flat b-wave for the given stimulus of 0.001 cd.s/m² for the measuring points of week 1 and week 2 and were consistent in most of the groups. However, this change does not indicate any irreversible functional impairment and was not consistent through other ERG parameters; therefore, a long-term damage effect cannot be assumed.

In vivo retinal imaging

Hyper-FAF changes were often found in a circular arrangement around the optic nerve head or in a patch or mottled fashion across the posterior pole. These deposits were located in the outer nuclear layer along the IS/OS junction and sometimes reached the outer segment layer in the OCT. The FAF changes became

weaker within 12 weeks and disappeared after 3 months, although subtle FAF changes remained in 2/4 eyes in the PEA group, 1/5 eyes in the PLGA group, and 4/4 eyes in the PEA+DEXA group. The circular pattern may be caused by the preference for transporting very small particles or parts of particles along optic nerve fibers in the direction of the optic nerve head in the process of degradation. We propose that the hyper-AF in FAF imaging and the hyper-reflective signal in OCT were caused by deposits rather than by tissue damage. Andrés-Guerrero et al. reported that, under fluorescence microscopy equipped with filters for fluorescence-emission spectra of 515/65 nm, 647/70 nm, and 445/45 nm, PEA microspheres had AF emission in the blue, green, and red spectral regions, respectively [19]. The PLGA microcapsules were found to have weak emission between 500 and 550 nm under excitation of 488 nm [30]. As the HRA+OCT Spectralis® device used in the present study employed a 488 nm laser for excitation and detected emitted light above 500 nm with a barrier filter for FAF, the device also might detect the AF from deposited material. Furthermore, most OCT abnormalities disappeared within 2 weeks, and a normal intact retinal layer reappeared as soon as these abnormalities disappeared. There was no swelling, atrophy, disappearance, or disruption of the retinal layer at month 3; therefore, it can be concluded that no damage occurred. In the ring scan of OCT, we did not notice a significant change of retinal thickness in any group.

Histology

PEA microspheres can lose their shape or dissolve when in contact with xylene, ethanol, or acetone during the dehydration steps required for paraffin and epoxy resin embedding techniques [19]. Ethanol has also been found to change the

surface, pore size, and structure of PLGA [31]. The in-vitro degradation in PBS is very slow when the polymer degrades in presence of enzymes. In vivo degradation of the polymer does not match the in-vitro rate [11,14,20,21,23]. For histologic preparation in this study, the eyes were fixed in paraformaldehyde (for light microscopy) and glutaraldehyde (for electron microscopy), as described by Andrés-Guerrero et al., and cryosectioned for tissue preparation for immunohistochemistry. Microsphere particles were seen as red dots in GFAP and IBA staining. In TEM, degradation remnants and empty spaces were observed inside and between retinal cells. Compared with the mean particle sizes of PEA (10–20 µm) and PLGA (20 µm) [19], the remnants of materials and empty spaces inside or between cells were very small (about 2–3 µm) and did not affect the viability of retinal cells. Activated macrophages detected in the vitreous space near the inner limiting membrane (ILM) might be associated with the degradation of material. The empty space in TEM might be caused in part by washout effects of material by ethanol during the dehydration steps for tissue preparation. The PLGA group showed more pronounced Müller cell activation than the other groups in immunohistochemistry at 1 month and greater loss of the plasma membrane between two adjacent cells in TEM at 3 months. These findings in immunohistochemistry and TEM could imply cellular damage even though there was no sign of increased cell death in TUNEL staining or significant functional changes in ERG. The PEA microspheres loaded with dexamethasone showed less pronounced Müller cell and microglial cell activation in both GFAP and IBA staining, indicating the protective effect of dexamethasone. Glial cell activation is a quite common reaction to intravitreal injection itself [32,33,34,35]. Müller cells are important for preserving normal retinal function and protect the tissue from injuries

[36]. Similar to Müller cells, the reactivation of astrocytes (astrogliosis) also occurs in response to nervous system damage [37]. Reactive gliosis includes morphological, biochemical, and physiological changes of Müller cells [32,39]. An important mechanism is increased expression of the intermediate filaments GFAP, vimentin, and nestin, which is a crucial step for the gliotic response [35,38]. Such changes do not necessarily indicate pathology but may represent a physiological response that does not indicate toxicological events. However, gliosis is also associated with functional changes in Müller cell such as glycolysis, potassium flow, and water clearance, which result in edema and neuron hyperexcitability caused by glutamate toxicity [32,36,40,41]. In gliosis the potassium extraction of Müller cell membranes decreases dramatically [40], which would change the ERG responses. In the present study, no significant change was observed in the ERG response, implying that no dramatic change in potassium extraction [40] occurred in Müller cells. Moreover, the FAF change and OCT deposits tended to disappear by month 3, which suggested a reversible non-toxic effect. This was also supported by the lack of swelling in OCT and histology results indicating that no glutamate toxicity occurred [32,36,40,41].

In summary, prominent adverse effects were not detected 3 months after intravitreal injection of microspheres compared to untreated eyes. Although hyper-FAF and abnormal deposits were detected in the FAF and OCT images, most changes were resolved at month 3, and there was no significant change in rod or cone amplitude or implicit times in ERG. TEM imaging showed that the majority of microsphere particles were degraded, leaving tiny remnants or empty spaces in the retinal and RPE cells or basolateral space between RPE cells in all injected groups, although minor cell damage was observed in the PLGA group at month 3. Further

studies with a longer period of observation, dose escalation, different microsphere sizes, and different sites of injection (e.g., intravitreal vs. subretinal vs. suprachoroidal) will be needed to ascertain the safety of these drugs.

Acknowledgments

PANOPTES is the acronym of a research project entitled ‘Peptide-based Nanoparticles as Ocular Drug Delivery Vehicles.’ The project is supported by funding from the Nanosciences, Nanotechnologies, Materials & New Production Technologies (NMP) Theme of the Cooperation Program, under the 7th Research Framework Program of the European Union (grant agreement number NMP4-SL-2010-246180). Tistou and Charlotte Kerstan Foundation, Deutsche Forschungsgemeinschaft (DFG) EXC 307

Reference

1. Herrero-Vanrell R, Bravo-Osuna I, Andrés-Guerrero V, Vicario-de-la-Torre M, Molina-Martínez IT.

The potential of using biodegradable microspheres in retinal diseases and other intraocular pathologies.

Prog Retin Eye Res. 2014;42:27-43.

2. Yihan Xu, Chang-Soo Kim, David M. Saylor and Donghun Koo

Polymer degradation and drug delivery in PLGA-based drug–polymer applications: A review of experiments and theories.

Article first published online: 21 APR 2016 | DOI: 10.1002/jbm.b.33648

3. Tan DT, Chee SP, Lim L, Theng J, Van Ede M.

Randomized clinical trial of Surodex steroid drug delivery system for cataract surgery: anterior versus posterior placement of two Surodex in the eye. Ophthalmology. 2001;108:2172-2181.

4. Haller JA, Bandello F, Belfort R Jr, et al.

Randomized, sham-controlled trial of dexamethasone intravitreal implant in patients with macular edema due to retinal vein occlusion.

Ophthalmology. 2010;117:1134-1146.e3.

5. Lowder C, Belfort R Jr, Lightman S, et al.

Dexamethasone intravitreal implant for noninfectious intermediate or posterior uveitis.

Arch Ophthalmol. 2011;129:545-553.

6. Srour M, Querques G, Leveziel N, et al.

Intravitreal dexamethasone implant (Ozurdex) for macular edema secondary to retinitis pigmentosa.

Graefes Arch Clin Exp Ophthalmol. 2013;251:1501-1506.

7. Campochiaro PA, Brown DM, Pearson A, et al.

Sustained delivery fluocinolone acetonide vitreous inserts provide benefit for at least 3 years in patients with diabetic macular edema.

Ophthalmology. 2012;119:2125-2132.

8. Calvo P, Ferreras A, Al Adel F, Wang Y, Brent MH.

Dexamethasone intravitreal implant as adjunct therapy for patients with wet age-related macular degeneration with incomplete response to ranibizumab.

Br J Ophthalmol. 2015;99:723-726.

9. Kunou N, Ogura Y, Yasukawa T, et al.

Long-term sustained release of ganciclovir from biodegradable scleral implant for the treatment of cytomegalovirus retinitis.

J Control Release. 2000;68:263-271.

10. Sun H, Meng F, Dias AA, Hendriks M, Feijen J, Zhong Z

α-Amino acid containing degradable polymers as functional biomaterials: rational design, synthetic pathway, and biomedical applications.

Biomacromolecules. 2011 Jun 13;12(6):1937-55. doi: 10.1021/bm200043u. Epub 2011 Apr 26.

11. Katsarava R, Beridze Z, Arabuli N, et al.

Amino acid-based bioanalogous polymers. Synthesis, and study of regular poly(ester amide)s based on bis(α-amino acid) α,ω-alkylene diesters, and aliphatic dicarboxylic acids.

J Polym Sci, Part A: Polym Chem. 1999:37;391-407.

12. Jiaolong Lv,, Huanli Sun, Yan Zou, Fenghua Meng, Aylvin A. Dias, Marc Hendriks,

Jan Feijen and Zhiyuan Zhong

Reductively degradable α-amino acid-based poly(ester amide)-graft-galactose copolymers: facile synthesis, self-assembly, and hepatoma-targeting doxorubicin delivery.

Biomater. Sci., 2015,3, 1134-1146, DOI: 10.1039/C4BM00436A, Received 16 Dec 2014, Accepted 19 Mar 2015, First published online 08 Apr 2015

13. Nicolas J, Mura S, Brambilla D, et al.

Functionalization strategies and biomedical applications of targeted biodegradable/biocompatible polymer-based nanocarriers for drug delivery.

Chem Soc Rev. 2013:42;1147-1235.

14. Tsitlanadze G1, Machaidze M, Kviria T, Djavakhishvili N, Chu CC, Katsarava R

Biodegradation of amino-acid-based poly(ester amide)s: in vitro weight loss and preliminary in vivo studies.

J Biomater Sci Polym Ed. 2004;15(1):1-24.

15. Pang X, Chu CC.

Synthesis, characterization and biodegradation of functionalized amino acid-based poly(ester amide)s.

Biomaterials. 2010:31;3745-3754.

16. Kropp M, Morawa K-M, Mihov G, et al.

Biocompatibility of Poly(ester amide) (PEA) Microfibrils in Ocular Tissues.

Polymers. 2014:6;243-260.

17. Webster M1, Harding S, McClean D, Jaffe W, Ormiston J, Aitken A, Watson T.

First-in-human evaluation of a sirolimus-eluting coronary stent on an integrated delivery system: the DIRECT study.

EuroIntervention. 2013 May 20;9(1):46-53. doi: 10.4244/EIJV9I1A8.

18. Brunner A, Mäder K, Göpferich A.

pH and osmotic pressure inside biodegradable microspheres during erosion.

Pharm Res. 1999:16;847-853

19. Andrés-Guerrero V, Zong M, Ramsay E, et al.

Novel biodegradable polyesteramide microspheres for controlled drug delivery in Ophthalmology.

J Control Release. 2015;211: 105-117

20. Freitas S, Merkle H, Gander B.

Microencapsulation by solvent extraction/evaporation: reviewing the state of the art of microsphere preparation process technology.

J Control Release. 2005:102;313-332.

21. Arabuli, N., Tsitlanadze, G., Edilashvili, L., Kharadze, D., Goguadze, T., Beridze, V., Gomurashvili, Z., Katsarava, R.

Heterochain polymers based on natural amino acids. Synthesis and enzymatic hydrolysis of regular poly(ester amide)s based on bis(L-phenylalanine) apalkylene diesters and adipic acid.

Macromol. Chem. Phys. 1994, 195, 2279–2289.

22. Ghaffar A., Draaisma G., Mihov G., Dias A., Schoenmakers P., Van Der Wal Sj.,

Monitoring the in vitro enzyme-mediated degradation of degradable poly(ester amide) for controlled drug delivery by LC-ToF-MS.

Biomacromolecules. 2011 Sep 12;12(9):3243-51.

23. Tsitlanadze G, Kviria T, Katsarava R

In vitro enzymatic biodegradation of amino acid based poly(ester amide)s

biomaterials

Journal of Material science in Medicine 15 (2004) 185-190

24. Strasser T, Wilke R, Messias A, Zrenner E.

Erg explorer: a software for post-processing, analysing, and reporting of electrophysiological data.

Acta Ophthalmologica, 2008:86(s243);0.

25. Strasser T, Peters T, Jagle H, Zrenner E, Wilke R.

An integrated domain specific language for post-processing and visualizing electrophysiological signals in Java.

Conf Proc IEEE Eng Med Biol Soc. 2010;2010:4687-4690.

26. Tröger E.

Assessment of Morphology and Function in Retinal Degeneration by Multi-Modal Mapping.

1st ed. Aachen, Germany: Shaker verlag; 2011:48-55.

27. Dhillon H1, Kalra SP, Prima V, Zolotukhin S, Scarpace PJ, Moldawer LL, Muzyczka N, Kalra PS.

Central leptin gene therapy suppresses body weight gain, adiposity and serum insulin without affecting food consumption in normal rats: a long-term study.

Regul Pept. 2001 Jun 15;99(2-3):69-77.

28. Ferry, E. L. (1913)

The rate of growth of the albino rat.

Anat. Rec., 7: 433–441. doi: 10.1002/ar.1090071203

29. Frederick T. Fraunfelder,Frederick W. Fraunfelder Jr.,Wiley A. Chambers

Clinical Ocular Toxicology: Drug-Induced Ocular Side Effects.

ISBN-13: 978-0323319843

30. Gong A, Ma X, Xiang L, et al.

Improved double emulsion technology for fabricating autofluorescent microcapsules as novel ultrasonic/fluorescent dual-modality contrast agents.

Colloids Surf B Biointerfaces. 2014;116:561-567.

31. Shearer H, Ellis MJ, Perera SP, Chaudhuri JB.

Effects of common sterilization methods on the structure and properties of poly(D,L lactic-co-glycolic acid) scaffolds.

Tissue Eng. 2006;12:2717-2727.

32. Bringmann A, Pannicke T, Grosche J, et al.

Müller cells in the healthy and diseased retina.

Prog Retin Eye Res. 2006;25:397-424.

33. Seitz R, Tamm ER.

Müller cells and microglia of the mouse eye react throughout the entire retina in response to the procedure of an intravitreal injection.

Adv Exp Med Bio. 2014;801:347-53.

34. Bringmann A, Pannicke T, Moll V, et al.

Upregulation of P2X7 receptor currents in Müller glial cells during proliferative vitreoretinopathy.

Invest Ophthalmol Vis Sci. 2001;42:860-867.

35. Lewis GP, Fisher SK.

Up-regulation of glial fibrillary acidic protein in response to retinal injury: its potential role in glial remodeling and a comparison to vimentin expression.

Int Rev Cytol. 2003;230:263-290.

36. Bringmann A, Pannnicke T, Biedermann B, et al.

Role of retinal glial cells in neurotransmitter uptake and metabolism.

Neurochem Int. 2009;53:143-160.

37. Sofroniew MV.

Reactive astrocytes in neural repair and protection.

Neuroscientist. 2005;11:400-407.

38. Lewis GP, Guerin CJ, Anderson DH, Matsumoto B, Fisher SK.

Rapid changes in the expression of glial cell proteins caused by experimental retinal detachment.

39. Bringmann A, Reichenbach A, Wiedemann P.

Pathomechanisms of cystoid macular edema.

Ophthalmic Res. 2004;36:241-249.

40. Bringmann A, Francke M, Pannicke T, et al.

Role of glial K(+) channels in ontogeny and gliosis: a hypothesis based upon studies on Müller cells.

Glia. 2000;29:35-44

41. Tenckhoff S, Hollborn M, Kohen L, et al.

Diversity of aquaporin mRNA expressed by rat and human retinas.

Neuroreport. 2005;16:53-56.